Supporting Information

In Situ Deprotection of Polymeric Binders for Solution-Processible Sulfide-Based All-Solid-State Batteries

Jieun Lee, Kyulin Lee, Taegeun Lee, Hyuntae Kim, Kyungsu Kim, Woosuk Cho, Ali Coskun, Kookheon Char, and Jang Wook Choi**

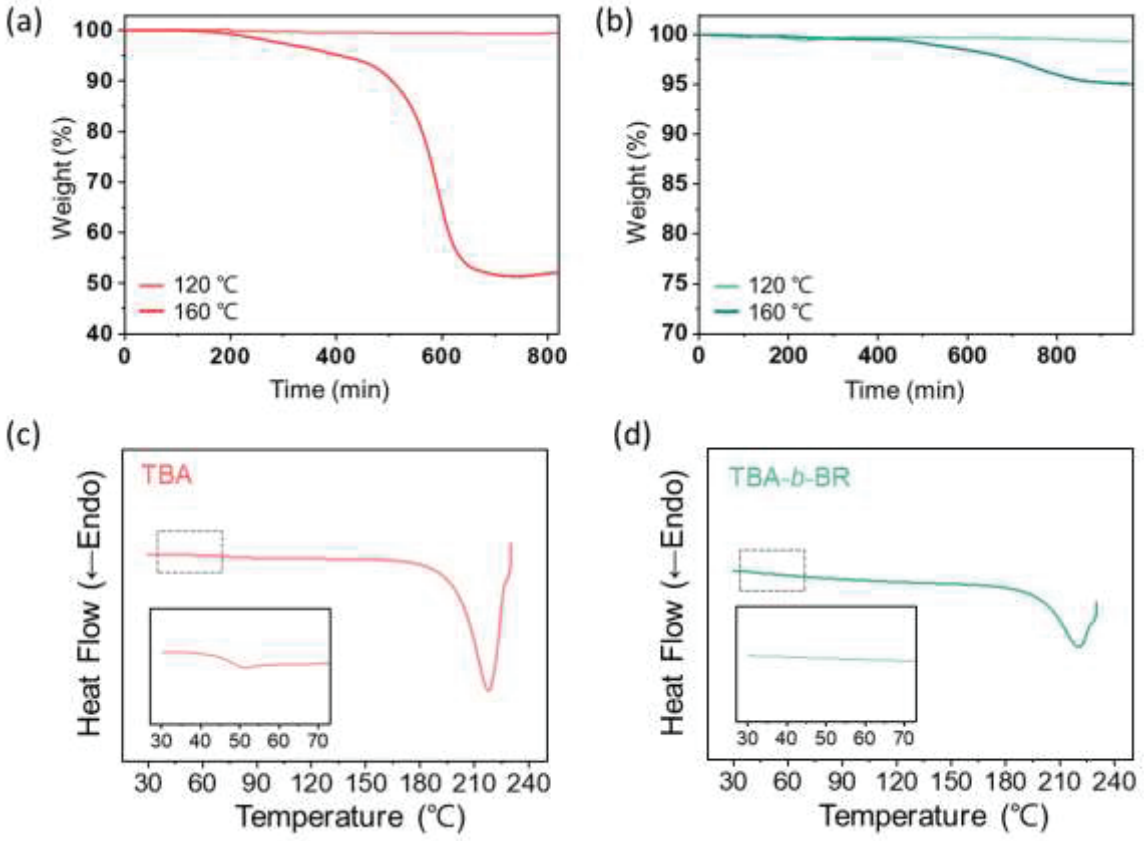

Figure S1. Isothermal TGA curves of (a) TBA and (b) TBA-*b*-BR binders with respect to the time at constant temperatures of 120 °C and 160 °C. DSC heating curves of (c) TBA and (d) TBA-*b*-BR recorded at a heating rate of 10 °C min^{-1}.

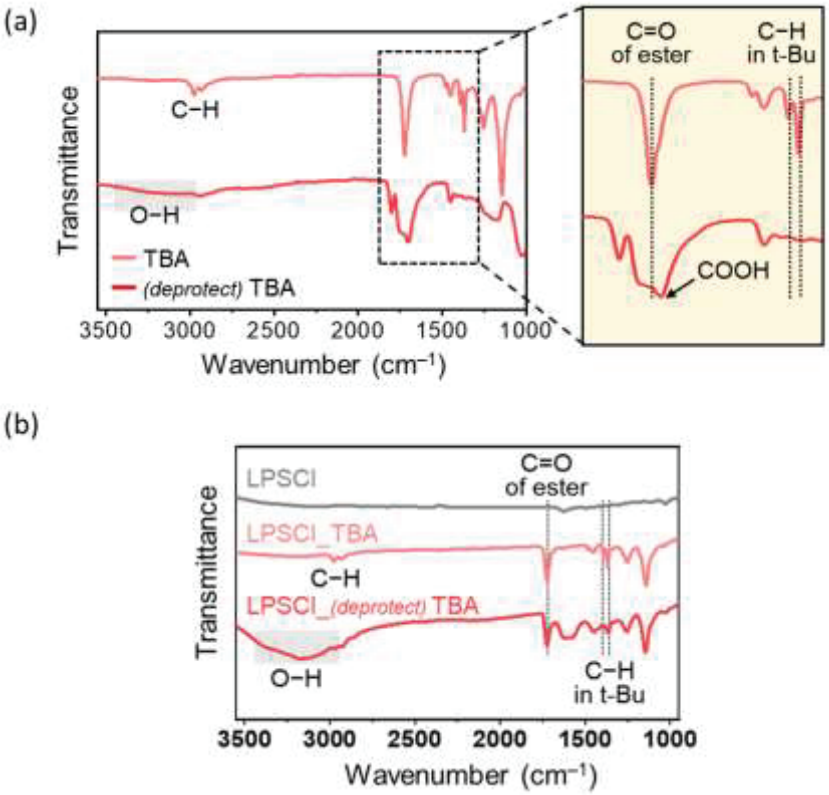

Figure S2. (a) FT-IR (ATR) spectra of TBA and *(deprotect)* TBA. (b) FT-IR (ATR) spectra of LPSCl solid electrolyte containing TBA binder (50 wt%) before and after the deprotection reaction.

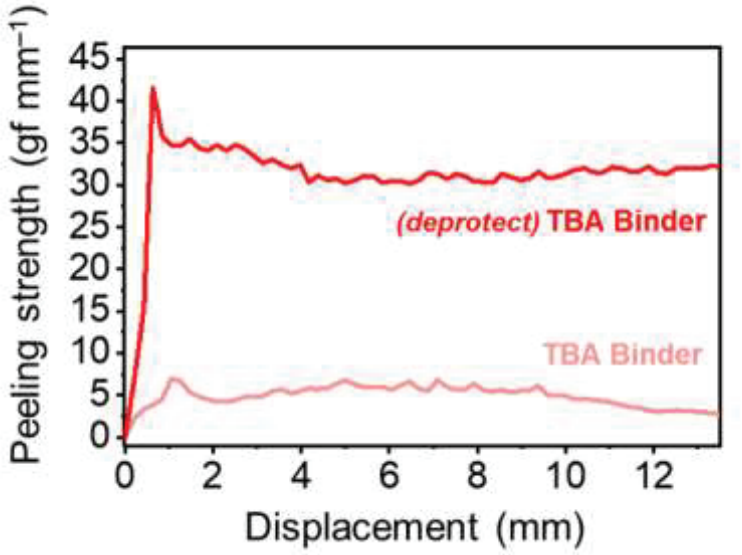

Figure S3. 180° peeling test results for films consisting of binder alone: TBA and *(deprotect)* TBA.

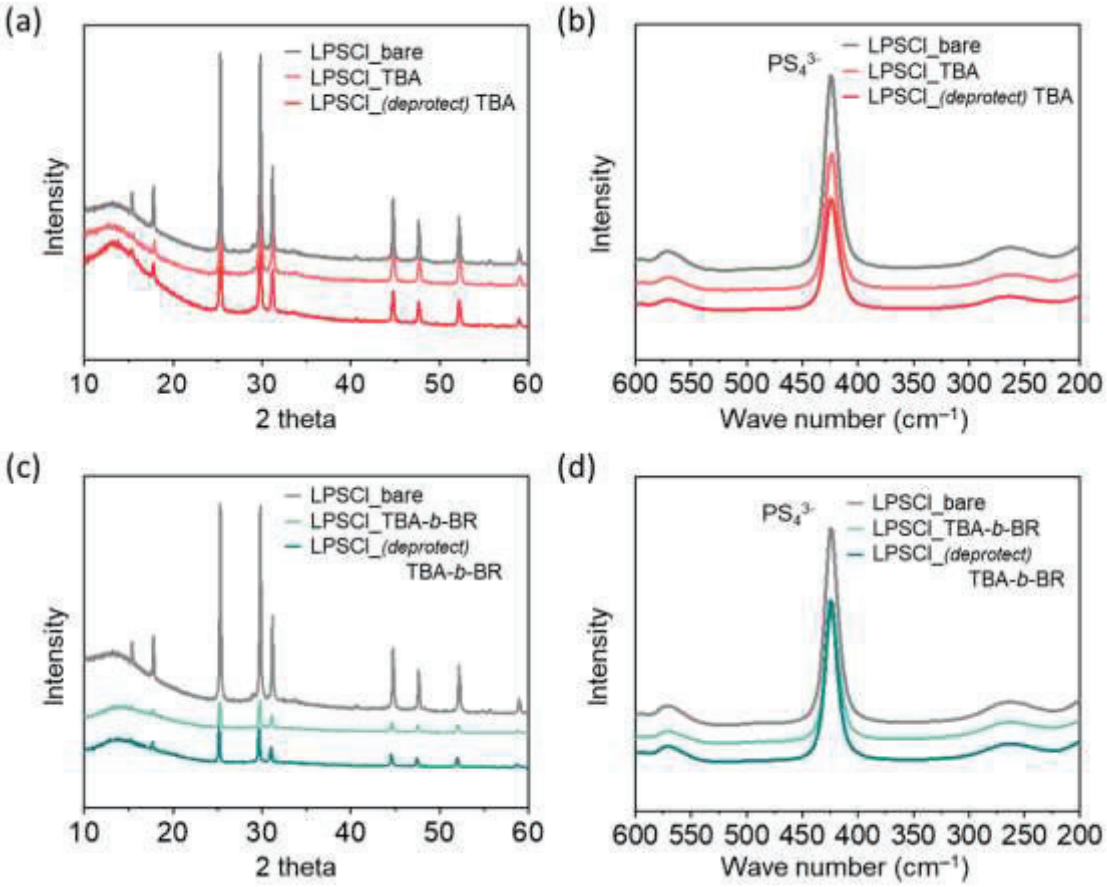

Figure S4. (a) XRD patterns and (b) Raman spectra of the bare argyrodite LPSCl SE and LPSCl SE after being immersed in TBA solution followed by drying at 120 °C or 160 °C for 15 h. (c) XRD patterns and (d) Raman spectra of the bare argyrodite LPSCl SE and LPSCl SE after being immersed in TBA-*b*-BR solution followed by drying at 120 °C or 160 °C for 15 h.

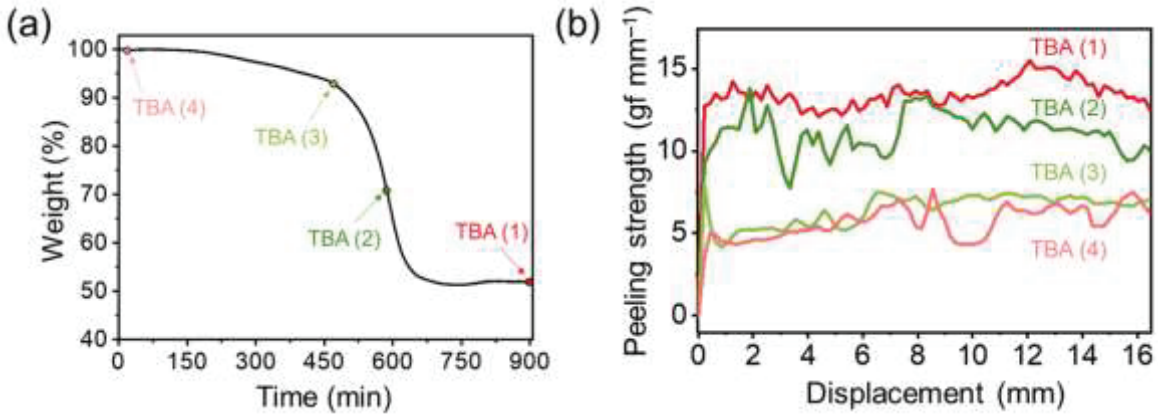

Figure S5. (a) Electrodes with different deprotection time as marked in the corresponding TGA profile and (b) their 180° peeling test results.

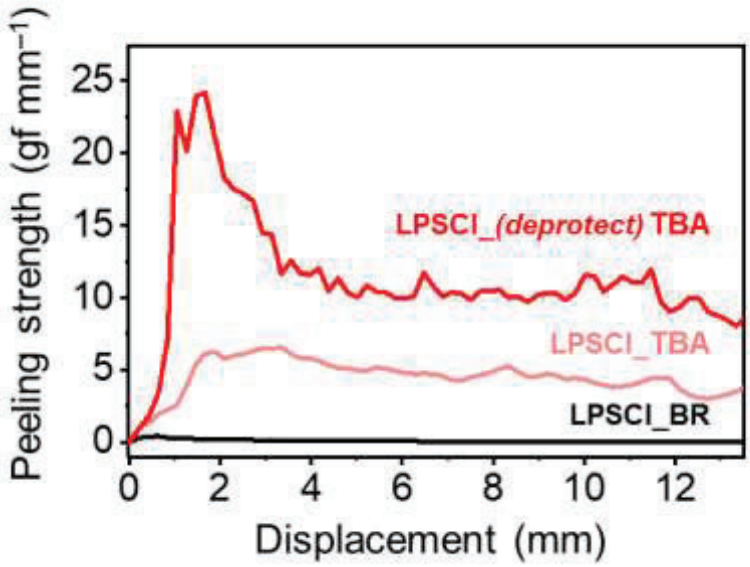

Figure S6. 180° peeling test results of LPSCl films containing different binders (10 wt%): *(deprotect)* TBA and BR.

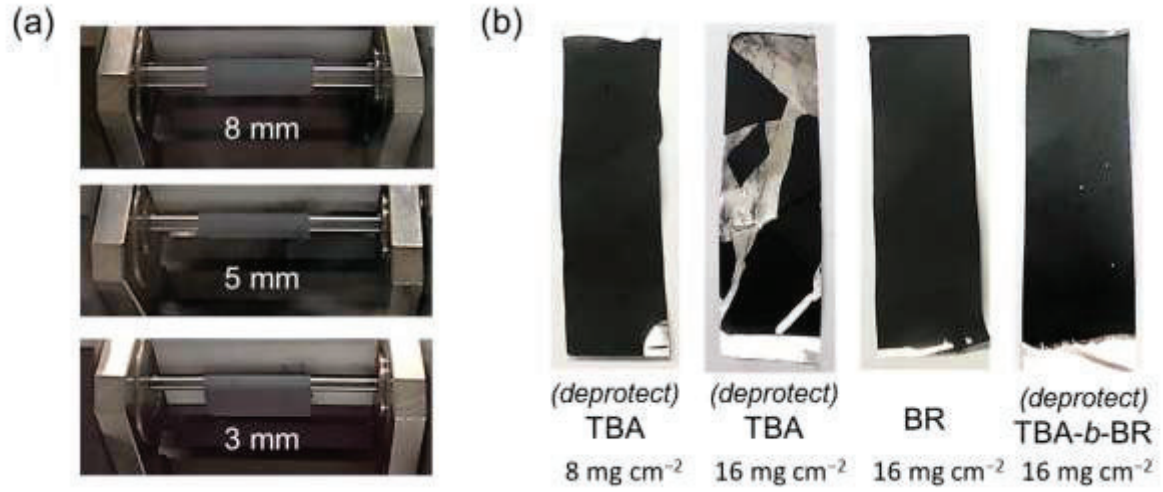

Figure S7. (a) Mandrel bending tests using cylindrical mandrels with different diameters. (b) Photographs of the composite cathodes containing different binders after bending tests with mandrels of different diameters.

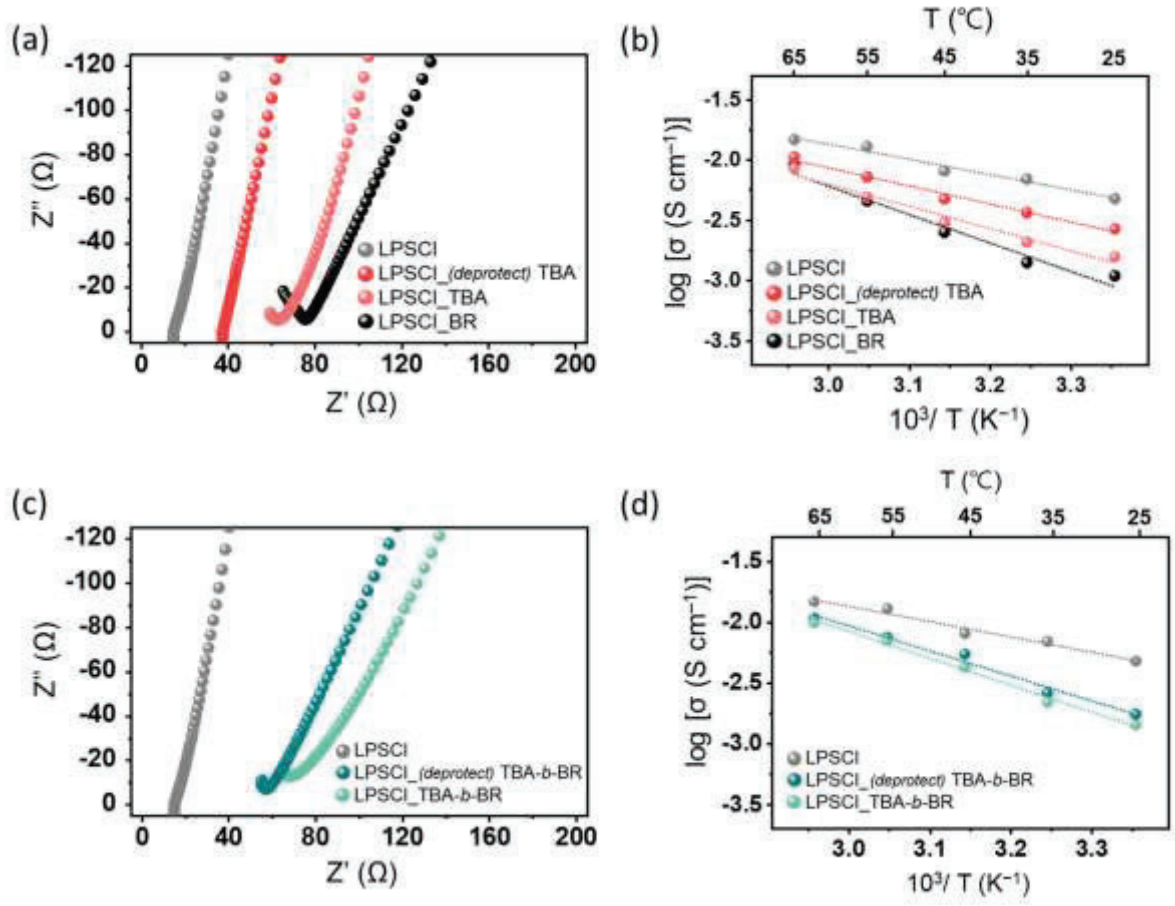

Figure S8. (a) Nyquist plots at 25 °C and (b) Arrhenius plots of lithium ion conductivities for the bare LPSCl and LPSCl solid electrolyte composite films containing TBA, *(deprotect)* TBA, and BR binders. (c) Nyquist plots at 25 °C and (d) Arrhenius plots of lithium ion conductivities for the bare LPSCl and LPSCl solid electrolyte composite films containing TBA-*b*-BR and *(deprotect)* TBA-*b*-BR binders.

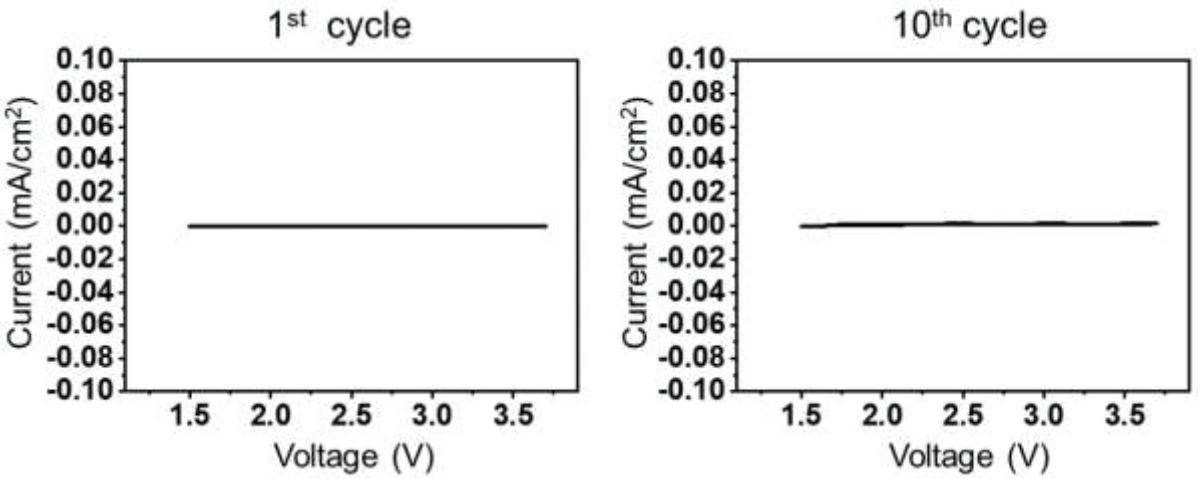

Figure S9. CV profiles of the *(deprotect)* TBA-*b*-BR film at the 1st and 10th cycles when measured at 0.1 mV s^{-1} in the potential range of 1.5–3.7 V *vs*. Li-In.

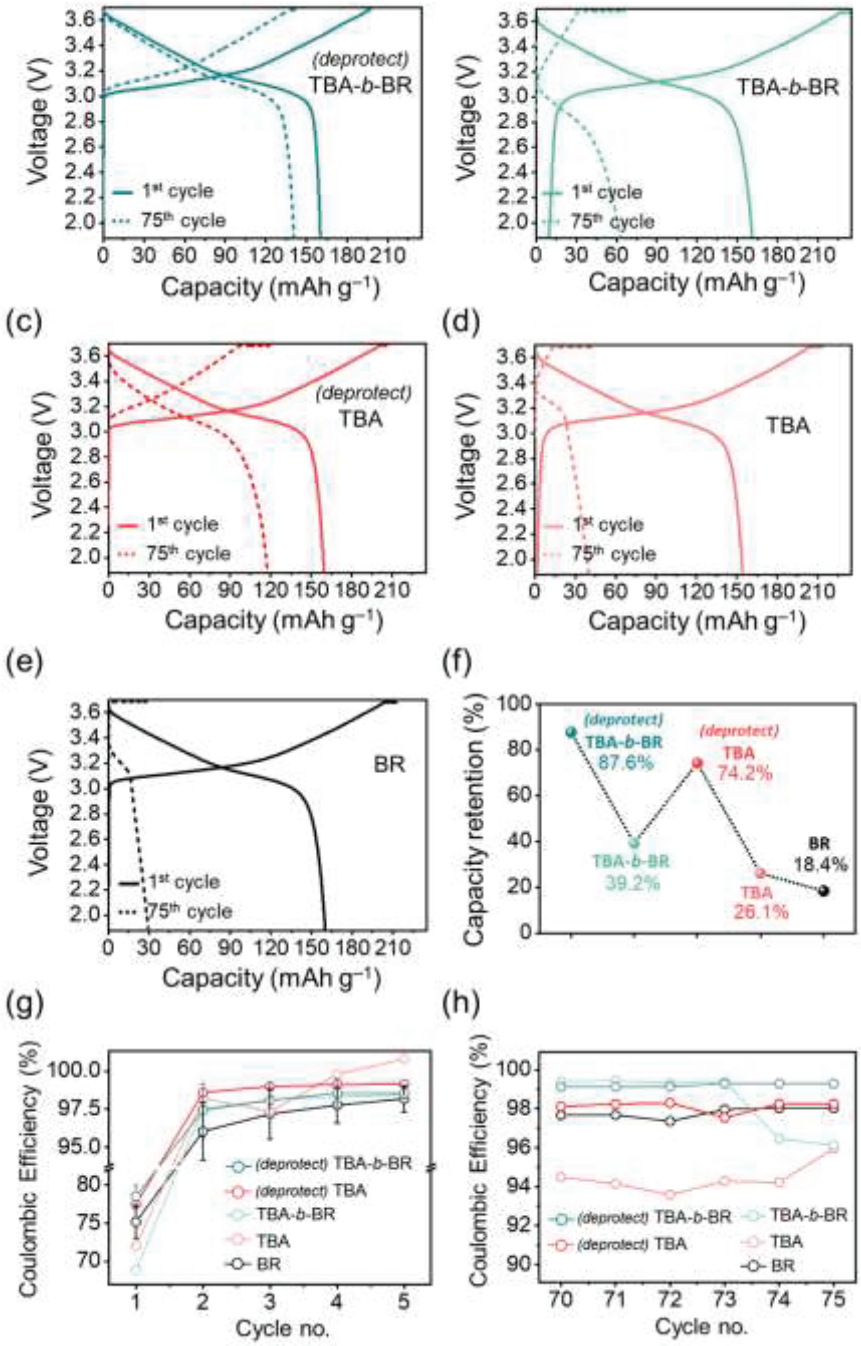

Figure S10. (a–e) 1st and 75th charge-discharge voltage profiles of the NCM/Li-In all-solid-state half-cells containing different binders when tested at 0.1C (19.5 mA g⁻1) at 25 °C. The areal loading of NCM711 active material = 8 mg cm^{-2}. (f) Capacity retentions of the same cells after 75 cycles. Coulombic efficiencies of (g) the first 5 cycles and (h) the last 5 cycles of the same cells when tested at 0.1C (19.5 mA g^{-1}) at 25 °C. The CE of the *(deprotect)* TBA-*b*-BR and BR cells in (g) are the averaged values from five independent measurements and the error bars indicate the standard deviations.

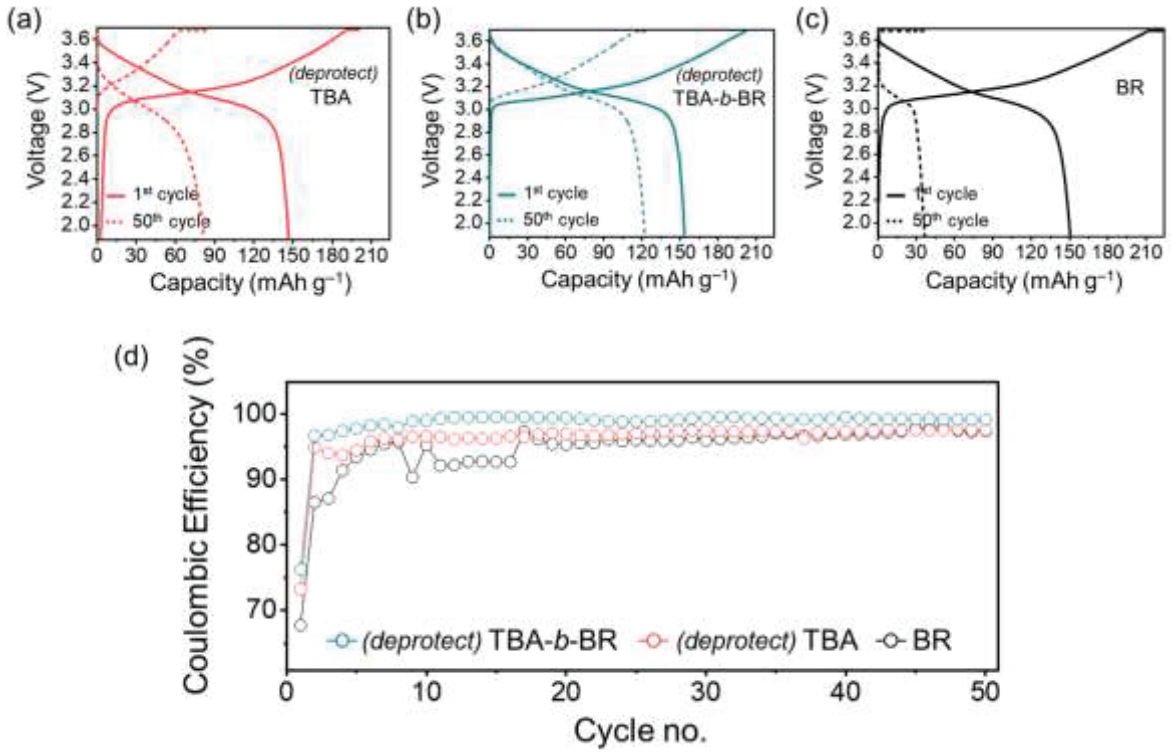

Figure S11. (a–c) Charge-discharge voltage profiles of the NCM/Li-In all-solid-state half-cells containing *(deprotect)* TBA, *(deprotect)* TBA-*b*-BR, and BR binders at the 1st and 50th cycles when tested at 0.1C (19.5 mA g^{-1}) at 25 °C. The areal loading of NCM711 active material = 16 mg cm^{-2}. (d) Coulombic efficiencies of the same cells during cycling.

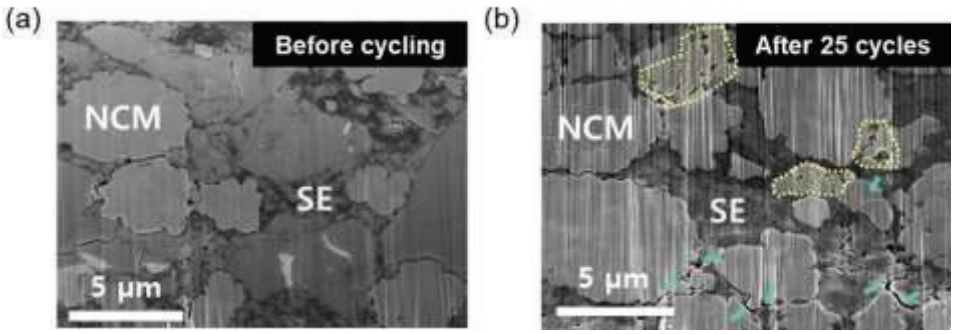

Figure S12. Cross-sectional SEM images of the composite cathode layers containing TBA-*b*-BR binder. (a) Before cycling and (b) after 25 charge-discharge cycles at 0.1C.

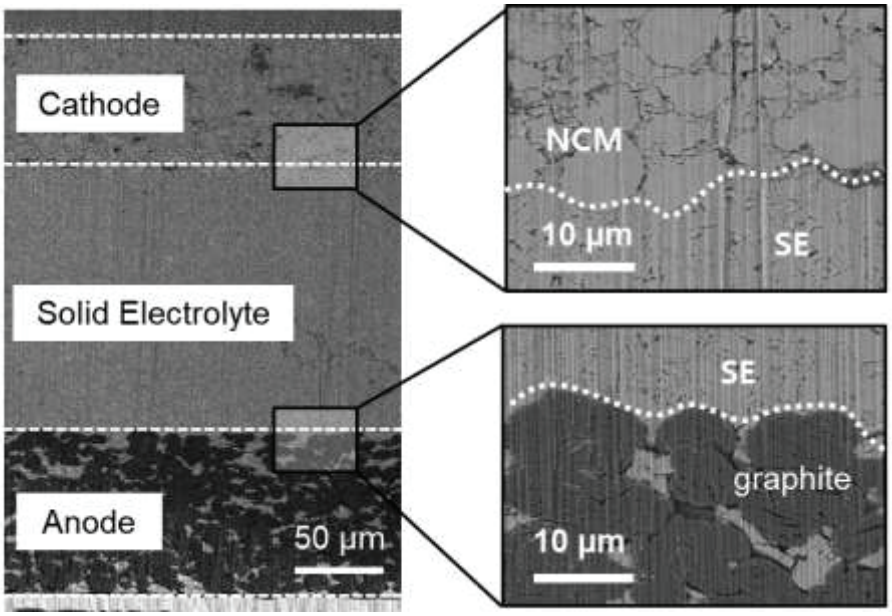

Figure S13. Cross-sectional SEM image of the NCM/graphite ASSB full-cell.

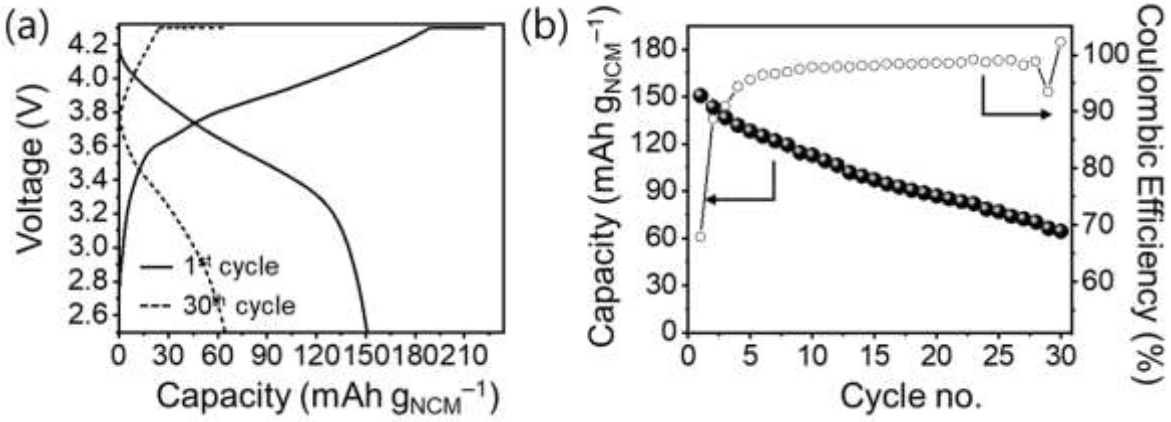

Figure S14. (a) 1st and 30th charge-discharge profiles of the NCM/graphite all-solid-state full-cell containing BR binder at 0.1C (19.5 mA g_{NCM}^{-1}) at 25 °C. Areal loading of NCM711 active material = 16 mg cm^{-2}. (b) Cycling performance and Coulombic efficiencies of the same full-cell in (a) when measured at 0.1C for both charge and discharge.